IOPscience iopscience.iop.org

Home Search Collections Journals About Contact us My IOPscience

Phonon–photon-assisted tunnelling through an Aharonov–Bohm ring

This article has been downloaded from IOPscience. Please scroll down to see the full text article.

2007 J. Phys.: Condens. Matter 19 226211

(http://iopscience.iop.org/0953-8984/19/22/226211)

View the table of contents for this issue, or go to the journal homepage for more

Download details:
IP Address: 129.252.86.83
The article was downloaded on 28/05/2010 at 19:08

Please note that terms and conditions apply.

IOP PUBLISHING JOURNAL OF PHYSICS: CONDENSED MATTER

J. Phys.: Condens. Matter **19** (2007) 226211 (14pp) doi:10.1088/0953-8984/19/22/226211

Phonon–photon-assisted tunnelling through an Aharonov–Bohm ring

Dongkwan Shin, Hüseyin Oymak and Jongbae Hong

Department of Physics and Astronomy, Seoul National University, Seoul 151-747, Korea

E-mail: dkshin1@snu.ac.kr

Received 16 January 2007, in final form 13 March 2007
Published 8 May 2007
Online at stacks.iop.org/JPhysCM/19/226211

Abstract

We model a four-site tight-binding Aharonov–Bohm (AB) ring whose sites house dispersionless Einstein phonons. The resonant tunnelling of an electron through the AB ring in the presence of a time-periodic magnetic flux which threads the ring is investigated. The Floquet scattering approach is followed within the electron–phonon Fock space. The Ricatti matrix method, a nonperturbative pruning technique, is utilized to extract the transmission properties of the system from the time-dependent Schrödinger equation. We observe additional satellite peaks in the total transmission graphs representing the photon-assisted tunnelling, as well as side resonances due to the phonon-assisted tunnelling. There happen to exist unusually stiff main transmission peaks that are not disturbed by the strong time-periodic magnetic flux, a finding attributed to the geometric characteristics of the AB ring.

1. Introduction

Recent advances in nanotechnologies have directed scientific attention to the study of the electron transport through very small mesoscopic structures, such as a quantum dot, quantum wire, and Aharonov–Bohm (AB) ring. In these systems, whose geometrical dimensions are much smaller than the elastic mean free path, electrons are transported ballistically and many interesting quantum coherent phenomena are observed [1]. As a standard method for probing the coherence, many experimentalists have made use of AB interferometers, and recently there has been a growing interest in hybrid systems composed of an AB interferometer and quantum dots [2–5]. One of the motivations for our work comes from the fact that it is possible at the present to embed quantum dots in the arms of AB rings, and perform quantum interference experiments in such systems [4, 5]. Electron waves on the dots scatter, leading a phase shift which is additional to the usual interference of the waves from the upper and lower part of the ring.

With the rapid progress of miniaturization, molecular electronics has become a subject of special interest in many branches of physics, chemistry, and biology [6]. A recent molecular

 © 2007 IOP Publishing Ltd Printed in the UK

experiment [7] reports that molecular vibrations significantly affect the electron transport through a single molecule, so that electron–phonon interactions become more prominent in very small single-molecular systems. Similarly, there appear in the literature experiments with the aim of probing the role of inelastic scattering in electron transport through very small single-molecular devices and semiconductor quantum dots [8, 9]. Outcomes from these studies indicate that interactions between electrons and longitudinal optical phonons has substantial, rather than perturbational, effects on the transport properties of the mesoscopic device under question. Single-molecular devices, in particular, have low-energy vibrational modes because of their notable weak elastic parameters. When the electron tunnels through the device, the coupling between these modes and the device's electronic states gives rise to low-energy phonons which are readily excited even at low temperatures [8–10]. This occurrence is referred to as phonon-assisted transport, and is one of the subjects of the present work. There have appeared many theoretical works on quantum transport in the presence of electron–phonon interaction; some notable examples are the treatments using the nonequilibrium Green function approach [11, 12], a study on the phonon-assisted tunnelling in a double-barrier resonant-tunnelling device [13], a work on the photon–phonon-assisted tunnelling through a single-molecule quantum dot [10], and inelastic transport studies in a variety of molecular systems [14–18]. The nonperturbative work of Bonča *et al* [19, 20] is of special importance; they resort to the mapping of a many-body problem onto an effective two-dimensional one-body problem with the number of phonons as the second dimension, and then obtain the transmission probability, within a Landauer's picture, using a recursive pruning method.

The electron transport through a nanoscale conductor which is driven by external sinusoidally alternating fields has been one of the most interesting subjects in recent years. An immediate example is photon-assisted tunnelling, also among the subjects of the present work, which has been widely investigated in a variety of mesoscopic systems [21, 22]. For a system under the effect of a time-periodic potential with an arbitrary strength and frequency, the Floquet approach [23–25] is especially the most convenient, for it provides essentially exact, i.e. nonperturbative, solutions. It has seemed that, however, the Floquet scattering approach is applicable only to effectively noninteracting Hamiltonians, and that it might not be generalized straightforwardly to a case with additional electron–phonon interaction [26].

In this work, we present a fully nonperturbative treatment for the phonon–photon-assisted tunnelling through an AB ring threaded by both static and oscillating magnetic fields. We build an electron–phonon Fock space [19, 20] to deal with electron–phonon interaction, enabling us to treat the system as a simple electronic tight-binding model with extra dimensions. Notwithstanding the fact that there exist electron–phonon interactions in the system, we shall demonstrate how to deal with the time-periodic external field by applying the Floquet theory to the interacting Hamiltonian under consideration. The following derivations are carried out for the system expanded within the electron–phonon Fock space, which is equivalent to an effectively noninteracting electron model. We make use of the Ricatti matrix method [27, 28] as the principal pruning technique to calculate the total transmission, which is given by the sum of the transmittances over the final phonon and Floquet channels. We shall be interested in three sequential cases: an AB ring (i) under the effect of only a time-periodic magnetic flux without electron–phonon interaction, (ii) in the presence of electron–phonon interaction with only a static flux but without a dynamic flux, and (iii) with all possible kinds of interaction.

2. Method and formulation

As is depicted in figure 1, the *system* under consideration is composed of a four-site AB *ring* ($0 \leqslant j \leqslant 3$) and semi-infinite left ($j < 0$) and right ($j > 3$) leads connected to the ring.

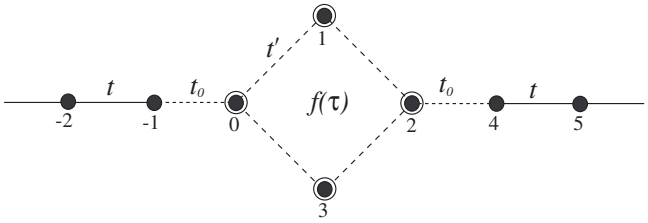

Figure 1. The system under study: a four-site AB ring connected to one-dimensional semi-infinite left and right leads. The sites of the ring house the same single Einstein phonon mode. A time-periodic magnetic flux $f(\tau)$ threads the ring. A dot with a circle describes a site coupled with the phonon mode.

Each site of the ring is coupled to the same single Einstein phonon mode, with a frequency Ω. We conceive that the ring is threaded by a time-periodic magnetic flux of period $p = 2\pi/\omega$, expressed in the units of the flux quantum h/e,

$$f(\tau) = f_{\rm s} + f_{\rm d}\cos\omega\tau, \tag{1}$$

where τ is the time variable, and $f_{\rm s}$ and $f_{\rm d}$ are, respectively, strengths of static and dynamic flux. An electron coming from the left lead is affected by both its interaction with the phonons and the time-periodic flux in the central part. We assume that electron–phonon interaction is restricted only to the sites of the ring, while the time-periodic flux influences the electron in the course of hopping from one site to the next within the ring. Both interactions are therefore described separately in the Hamiltonian of the system,

$$H(\tau) = H_{\rm L(R)} + H_{\rm AB}(\tau) + H_{\rm c} \tag{2}$$

with

$$H_{\rm L(R)} = \sum_j \epsilon_j c_j^\dagger c_j - t\sum_{\langle j,\ell\rangle}(c_j^\dagger c_\ell + {\rm H.c.}), \tag{3}$$

$$H_{\rm AB}(\tau) = \sum_j [\epsilon_j c_j^\dagger c_j + \Omega a_j^\dagger a_j - \kappa c_j^\dagger c_j (a_j^\dagger + a_j)] - t'\sum_{\langle j,\ell\rangle}[{\rm e}^{{\rm i}\pi f(\tau)/2} c_j^\dagger c_\ell + {\rm H.c.}], \tag{4}$$

$$H_{\rm c} = -t_0\sum_{\langle j,\ell\rangle}(c_j^\dagger c_\ell + {\rm H.c.}), \tag{5}$$

where $H_{\rm L(R)}$, $H_{\rm AB}$, and H_c represent the Hamiltonians of the left (right) lead, the ring, and the coupling of the leads to the ring, respectively. The operator $c_j^\dagger$ (c_j) creates (annihilates) an electron at site j with the onsite energy ϵ_j, and $a_j^\dagger$ (a_j) is the operator for the creation (annihilation) of a phonon at site j with the frequency Ω. The real constants t and t' respectively denote the hopping amplitude within the lead and the ring, and t_0 denotes that from leads to the central part. The electron–phonon interaction is mediated via the coupling strength κ. Finally 'H.c.' stands for Hermitian conjugate. Hereafter, for simplicity, all the onsite energies, ϵ_j, are set to zero.

We note that it is $f(\tau)$ that makes the Hamiltonian (2) time-periodic, i.e., $H(\tau) = H(\tau + p)$. The Floquet theory, then, asserts that the time-dependent Schrödinger equation, ${\rm i}|\dot\Psi(\tau)\rangle = H(\tau)|\Psi(\tau)\rangle$, has solutions of the form

$$|\Psi(\tau)\rangle = {\rm e}^{-{\rm i}E_{\rm F}\tau}|\phi(\tau)\rangle, \tag{6}$$

where $E_{\rm F}$ is the Floquet energy ranging from 0 to ω. Since it also obeys the same time

periodicity, $|\phi(\tau)\rangle = |\phi(\tau + p)\rangle$, the Floquet state $|\phi(\tau)\rangle$ can be readily expanded into a Fourier series,

$$|\phi(\tau)\rangle = \sum_{m=-\infty}^{\infty} \mathrm{e}^{-\mathrm{i}m\omega\tau}|\phi_m\rangle, \tag{7}$$

After loading all the time dependence on the exponential function, the so-called Floquet sideband states, $|\phi_m\rangle$, can now be further expanded into polaron eigenstates, which are the direct product of electronic states and the phonon Fock states,

$$|j, \{n\}\rangle = c_j^\dagger \prod_{i=0}^{3} \frac{(a_i^\dagger)^{n_i}}{\sqrt{n_i!}}|0\rangle, \tag{8}$$

where n_i is the number of phonons at site i, $\{n\}$ indicates the set of n_i, i.e., $\{n_0, n_1, n_2, n_3\}$, and $|0\rangle$ is the vacuum state. After carrying out the mentioned expansion, we obtain the assumed solutions (6) as

$$|\Psi(\tau)\rangle = \sum_{j,m,\{n\}} \mathrm{e}^{-\mathrm{i}(E_\mathrm{F}+m\omega)\tau}\phi^m_{j,\{n\}}|j, \{n\}\rangle. \tag{9}$$

The substitution of this solution into the time-dependent Schrödinger equation yields

$$H(\tau)\sum_{j,m,\{n\}} \mathrm{e}^{-\mathrm{i}(E_\mathrm{F}+m\omega)\tau}\phi^m_{j,\{n\}}|j, \{n\}\rangle = \sum_{j,m,\{n\}} (E_\mathrm{F} + m\omega)\,\mathrm{e}^{-\mathrm{i}(E_\mathrm{F}+m\omega)\tau}\phi^m_{j,\{n\}}|j, \{n\}\rangle. \tag{10}$$

In this equation the conserved quantity is the Floquet energy E_F, not the total energy, according to the Floquet theory. It is possible for an electron with energy $E = E_\mathrm{F} + m\omega$, which determines the Floquet energy within the range $[0, \omega)$, to occupy any one of the sidebands with an energy spacing of ω since all the infinite number of sidebands can be expressed as $E_m = E_\mathrm{F} + m\omega$. It is to be noted, however, that in the electron–phonon interaction case, the system conserves its total energy E. The energy conservation for the electron–phonon model is given by $E = \epsilon_\mathrm{in} + \Omega\sum_i n_i = \epsilon_\mathrm{out} + \Omega\sum_i n'_i$, where ϵ_in (ϵ_out) is the electron energy before (after) scattering. Hence the energy of the outgoing electron from a channel $\{n'\}$ to another one $\{n\}$ is given by $\epsilon_\mathrm{out} = \epsilon_\mathrm{in} + \Omega\sum_i(n_i - n'_i)$, and including the case in which the electron occupies the mth Floquet sideband we obtain

$$\epsilon_\mathrm{out} = E_\mathrm{F} + m\omega + \Omega\sum_i(n_i - n'_i). \tag{11}$$

Here ϵ_out is written, within the nearest-neighbour tight-binding scheme, in terms of $k^m_{\{n\}}$, i.e., the wavevector of the outgoing electron reflected to the left or transmitted to the right,

$$\epsilon_\mathrm{out} = -2t\cos k^m_{\{n\}}. \tag{12}$$

With the use of the Jacobi–Anger expansion, $\mathrm{e}^{\mathrm{i}z\cos\theta} = \sum_{q=-\infty}^{\infty} i^q J_q(z)\mathrm{e}^{\mathrm{i}q\theta}$, we write the left-hand side of equation (10) as

$$\begin{aligned}(H_\mathrm{L} + H_\mathrm{R})|\Psi(\tau)\rangle = -t\sum_{m,\{n\}} U_m(\tau)\Bigg(&\sum_{j=-\infty}^{-2}\phi^m_{j+1,\{n\}} + \sum_{j=-\infty}^{-1}\phi^m_{j-1,\{n\}} \\ &+ \sum_{j=4}^{\infty}\phi^m_{j+1,\{n\}} + \sum_{j=5}^{\infty}\phi^m_{j-1,\{n\}}\Bigg)|j, \{n\}\rangle,\end{aligned} \tag{13}$$

$$\begin{aligned}H_\mathrm{c}|\Psi(\tau)\rangle = -t_0\sum_{m,\{n\}} U_m(\tau)(&\phi^m_{-1,\{n\}}|0, \{n\}\rangle \\ &+ \phi^m_{0,\{n\}}|-1, \{n\}\rangle + \phi^m_{2,\{n\}}|4, \{n\}\rangle + \phi^m_{4,\{n\}}|2, \{n\}\rangle),\end{aligned} \tag{14}$$

$$H_{\rm AB}^{(\omega)}|\Psi(\tau)\rangle = -t' \sum_{\ell=-\infty}^{\infty} \sum_{m,\{n\}} \sum_{j=0}^{3} J_\ell(\delta_{\rm d}) U_{m-\ell}(\tau) \times (\mathrm{e}^{\mathrm{i}\delta_{\rm s}} \mathrm{i}^{\ell} \phi^m_{j,\{n\}} |j^+, \{n\}\rangle + \mathrm{e}^{-\mathrm{i}\delta_{\rm s}} (-\mathrm{i})^{\ell} \phi^m_{j^+,\{n\}} |j, \{n\}\rangle), \tag{15}$$

$$H_{\rm AB}^{(\Omega)}|\Psi(\tau)\rangle = \sum_{m,\{n\}} \sum_{j=0}^{3} U_m(\tau) \phi^m_{j,\{n\}} [\Omega \Sigma n |j, \{n\}\rangle - \kappa(\sqrt{n_j+1}|j, \{(n_j+1)\}\rangle - \sqrt{n_j-1}|j, \{(n_j-1)\}\rangle)], \tag{16}$$

with $\delta_{\rm s(d)} = \pi f_{\rm s(d)}/2$, $U_m(\tau) = \mathrm{e}^{-\mathrm{i}(E_{\rm F}+m\omega)\tau}$, $\Sigma n \equiv n_0 + n_1 + n_2 + n_3$, and $|j, \{(n_i+1)\}\rangle \equiv |j, \ldots, n_{i-1}, n_i + 1, n_{i+1}, \ldots\rangle$. Hamiltonians $H_{\rm AB}^{(\omega)}$ and $H_{\rm AB}^{(\Omega)}$ describe the effect of the time-periodic flux and the electron–phonon coupling, respectively. The site $j^{+(-)}$ is the nearest neighbour within the ring along the clockwise (counterclockwise) direction. Substituting equations (13)–(16) into (10) and operating with $\langle j', \{n'\}| \int \mathrm{d}\tau \mathrm{e}^{\mathrm{i}(E_{\rm F}+m'\omega)\tau}$ from the right, we finally obtain

$$\mathcal{E}^m_{\{n\}} \phi^m_{-1,\{n\}} = -t\phi^m_{-2,\{n\}} - t_0 \phi^m_{0,\{n\}}, \tag{17}$$

$$\mathcal{E}^m_{\{n\}} \phi^m_{0\leqslant j\leqslant 3,\{n\}} = -t_0(\delta_{j0}\phi^m_{-1,\{n\}} + \delta_{j2}\phi^m_{4,\{n\}}) - \sum_{\ell=-\infty}^{\infty} (\mathcal{P}_{\ell-m}\phi^{\ell}_{j^-,\{n\}} + \mathcal{P}^*_{\ell-m}\phi^{\ell}_{j^+,\{n\}}) - \kappa(\sqrt{n_j+1}\phi^m_{j,\{(n_j+1)\}} + \sqrt{n_j}\phi^m_{j,\{(n_j-1)\}}), \tag{18}$$

$$\mathcal{E}^m_{\{n\}} \phi^m_{4,\{n\}} = -t\phi^m_{5,\{n\}} - t_0 \phi^m_{2,\{n\}}, \tag{19}$$

with $\mathcal{E}^m_{\{n\}} = E_{\rm F} + m\omega - \Omega \sum_{i=0}^{3} n_i$ and $\mathcal{P}_{\ell-m} = t' J_{\ell-m}(\delta_{\rm d}) \mathrm{e}^{\mathrm{i}\delta_{\rm s}} \mathrm{i}^{\ell-m}$ being the energy in each channel and the hopping amplitude from the Floquet mode ℓ at site j^- to m at j within the ring, respectively. Equations (17)–(19) are expressed in compact matrix form as

$$\mathbf{E}\Phi_{-1} = -t\Phi_{-2} - t_0\Phi_0, \tag{20}$$

$$\mathbf{E}\Phi_0 = \mathbf{V}_0\Phi_0 - \mathbf{P}\Phi_3 - \mathbf{P}^*\Phi_1 - t_0\Phi_{-1}, \tag{21}$$

$$\mathbf{E}\Phi_1 = \mathbf{V}_1\Phi_1 - \mathbf{P}\Phi_0 - \mathbf{P}^*\Phi_2, \tag{22}$$

$$\mathbf{E}\Phi_2 = \mathbf{V}_2\Phi_2 - \mathbf{P}\Phi_1 - \mathbf{P}^*\Phi_3 - t_0\Phi_4, \tag{23}$$

$$\mathbf{E}\Phi_3 = \mathbf{V}_3\Phi_3 - \mathbf{P}\Phi_2 - \mathbf{P}^*\Phi_0, \tag{24}$$

$$\mathbf{E}\Phi_4 = -t_0\Phi_2 - t\Phi_5, \tag{25}$$

where any amplitude vector Φ_j is chosen as $(N_\Omega + 1)^4$ phonon submatrices and each such submatrix has $2N_\omega + 1$ elements, with N_Ω and N_ω being the maximum number of allowed phonons and (positive) Floquet sidebands, respectively, to be included in the numerical calculation. Eliminating Φ_1 and Φ_3 among the above equations, we obtain

$$\mathbf{E}\Phi_0 = \tilde{\mathbf{V}}_0\Phi_0 - \tilde{\mathbf{P}}_{02}\Phi_2 - t_0\Phi_{-1}, \tag{26}$$

$$\mathbf{E}\Phi_2 = \tilde{\mathbf{V}}_2\Phi_2 - \tilde{\mathbf{P}}_{20}\Phi_0 - t_0\Phi_4, \tag{27}$$

which, together with equations (20) and (25), designate a linear, nearest-neighbour tight-binding system with the effective potentials

$$\tilde{\mathbf{V}}_{0(2)} = \mathbf{V}_{0(2)} - \mathbf{P}[\mathbf{V}_{3(1)} - \mathbf{E}]^{-1}\mathbf{P}^* - \mathbf{P}^*[\mathbf{V}_{1(3)} - \mathbf{E}]^{-1}\mathbf{P} \tag{28}$$

and the effective hopping matrices

$$\tilde{\mathbf{P}}_{02(20)} = \mathbf{P}[\mathbf{V}_{3(1)} - \mathbf{E}]^{-1}\mathbf{P} + \mathbf{P}^*[\mathbf{V}_{1(3)} - \mathbf{E}]^{-1}\mathbf{P}^* \tag{29}$$

as depicted in figure 2. The solutions in the leads are conventionally written as

$$\phi^m_{j<0,\{n\}} = T^m_{{\rm L},\{n\}} \mathrm{e}^{\mathrm{i}k^m_{\{n\}}(j+1)} + R^m_{\{n\}} \mathrm{e}^{-\mathrm{i}k^m_{\{n\}}(j+1)}, \tag{30}$$

$$\phi^m_{j>3,\{n\}} = T^m_{{\rm R},\{n\}} \mathrm{e}^{\mathrm{i}k^m_{\{n\}}(j-4)}, \tag{31}$$

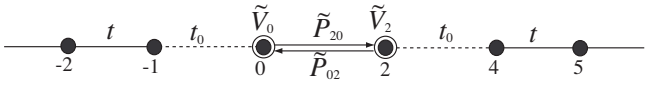

Figure 2. The transformed form of the problem under study in figure 1.

where $T^m_{\mathrm{L},\{n\}}$ is the probability amplitude of the incoming electron on the left lead, while $R^m_{\{n\}}$ and $T^m_{\mathrm{R},\{n\}}$ are those of the outgoing electron on the left and right leads, respectively. For future convenience we also express equations (30) and (31) in matrix form as

$$\mathbf{\Phi}_{j<0} = \mathbf{A}_j \mathbf{T}_{\mathrm{L}} + \mathbf{B}_j \mathbf{R}, \tag{32}$$

$$\mathbf{\Phi}_{j>3} = \mathbf{C}_j \mathbf{T}_{\mathrm{R}}, \tag{33}$$

where $\mathbf{A}_j$, $\mathbf{B}_j$, and $\mathbf{C}_j$ are diagonal matrices with the elements $\mathrm{e}^{\mathrm{i}k^m_{\{n\}}(j+1)}$, $\mathrm{e}^{-\mathrm{i}k^m_{\{n\}}(j+1)}$, and $\mathrm{e}^{\mathrm{i}k^m_{\{n\}}(j-4)}$, respectively.

Concerning a nearest-neighbour tight-binding problem like the one at hand, one can easily obtain the transmission and reflection amplitudes by exploiting the Ricatti ratio [27, 28] method, which is, in this work, generalized to a matrix method. We define a Ricatti matrix $\mathbf{Y}_j$ via

$$\mathbf{\Phi}_{j+1} = \mathbf{Y}_j \mathbf{\Phi}_j. \tag{34}$$

The application of this definition to the system shown in figure 2, together with equations (20), (25)–(29), results in a two-point recursion relation, called the Ricatti equation,

$$\mathbf{Y}_{j-1} = (\mathbf{V}_j - \mathbf{E} - \mathbf{t}_{j,j+1}\mathbf{Y}_j)^{-1}\mathbf{t}_{j,j-1}. \tag{35}$$

The initial datum needed is obtained with the aid of solutions (32) and (33) as

$$\mathbf{Y}_4 = \mathbf{C}_5. \tag{36}$$

It is important to notice that the hopping matrices between the two nearest-neighbour central sites are not equal, i.e., $\tilde{\mathbf{P}}_{02} \neq \tilde{\mathbf{P}}_{20}$. Taking into account the fact that $\mathbf{C}_4$ is the identity matrix, one obtains the expression for $\mathbf{T}_{\mathrm{R}}$ in terms of $\mathbf{T}_{\mathrm{L}}$ and $\mathbf{R}$ using equations (33) and (35) as

$$\mathbf{T}_{\mathrm{R}} = \mathbf{Y}_2\mathbf{Y}_0\mathbf{Y}_{-1}(\mathbf{T}_{\mathrm{L}} + \mathbf{R}), \tag{37}$$

and $\mathbf{R}$ in terms of $\mathbf{T}_{\mathrm{L}}$ using equations (32) and (35) as

$$\mathbf{R} = (\mathbf{I} - \mathbf{Y}_{-2}\mathbf{B}_{-2})^{-1}(\mathbf{Y}_{-2}\mathbf{A}_{-2} - \mathbf{I})\mathbf{T}_{\mathrm{L}}. \tag{38}$$

Using equation (38) in (37), one finally obtains the relation $\mathbf{T}_{\mathrm{R}} = \mathbf{t}\mathbf{T}_{\mathrm{L}}$, where $\mathbf{t}$ is the transmission amplitude matrix,

$$\mathbf{t} = \mathbf{Y}_2\mathbf{Y}_0\mathbf{Y}_{-1}(\mathbf{Y}_{-2}^{-1} - \mathbf{B}_{-2})^{-1}(\mathbf{A}_{-2} - \mathbf{B}_{-2}). \tag{39}$$

Since, in the numerical calculations, we should keep only those channels that propagate within the energy bands of the leads, we need to use only a submatrix of the transmission amplitude matrix (39). We designate such a submatrix by $\tilde{\mathbf{t}}$, whose elements $\tilde{t}_{\alpha\beta}$ give the transmission amplitude of an electron incident from a channel $\beta \equiv (m, \{n\})$ on the left lead to another one $\alpha \equiv (m', \{n'\})$ on the right lead. The transmission coefficient for an electron of energy $E = E_{\mathrm{F}} + m\omega - \Omega\Sigma n$ from the left to the right lead is then given by

$$T_\beta(E) = \sum_\alpha \frac{\sin k_\alpha}{\sin k_\beta} |\tilde{t}_{\alpha\beta}|^2 \tag{40}$$

with $k_\alpha \equiv k^{m'}_{\{n'\}}$ and $k_\beta \equiv k^m_{\{n\}}$. At a nonzero temperature $\mathcal{T}$, although we shall not expound on it in this work, a finite number $\{n\}$ of phonons will be already excited on each site of the

ring before the scattering, with a probability factor $P(\{n\}) = [1 - \mathrm{e}^{-\Omega/\mathcal{T}}]^4 \mathrm{e}^{-\Omega\Sigma n/\mathcal{T}}$. With the inclusion of this in the formalism, the total transmission is finally given by

$$T(E) = \sum_{\beta} P(\{n\}) T_{\beta}(E). \tag{41}$$

The method presented can be easily modified for similar continuous systems with or without electron–phonon interaction and/or any type of excitation. Two typical examples are those of Bulgakov *et al* [29] and Lubin *et al* [30]. They both consider a mesoscopic ring threaded by a time-dependent magnetic flux which is periodic in the former and linear in the latter; their systems do not contain any other interaction like electron–phonon interaction. For the moment, apart from their time dependence, our method appears capable of dealing with such *continuous* systems by simply taking the electron–phonon coupling constant as $\kappa = 0.0$ and choosing all hopping constants as $t = t' = t_0 = 1.0$ in order to make the tight-binding model at hand imitate its continuous counterpart. The time-periodicity of magnetic flux in this work, and in that of Bulgakov *et al* [29], is harmonic. If we are to be interested in the problem in which the time-periodic magnetic flux is pulsed, triangular, etc, we can readily use our method by first Fourier-expanding the magnetic flux, as Faizabadi *et al* [28] do. What about a magnetic flux which varies in time linearly, as in the work of Lubin *et al* [30]? Since time-periodicity is one of the main ingredients of this work, it seems not quite possible to apply the present method to such a system. Nevertheless, provided that the exposition of the magnetic flux is short in time, it *may* be possible to use the above method in such a system by taking the period of oscillation ω long enough and again by Fourier-expanding the magnetic flux. In this work we do not contemplate such issues further.

3. Results and discussion

In this section, we report some representative numerical outcomes for the total transmission (41) which is calculated using the Ricatti matrix method outlined above. In calculations the hopping amplitude within the leads sites is set to $t = 1.0$, and those among the ring sites and between the ring and leads to $t' = 0.5$ and $t_0 = 0.2$, respectively. We choose $N_\Omega = 5$ and $N_\omega = 10$ which are good enough for the results to converge with sufficient accuracy, so that the following discussions are all fully reliable.

We initially focus, in the absence of electron–phonon interaction ($\kappa = 0$), on the tunnelling under the effect of only a static flux, $f_\mathrm{s} \neq 0$ and $f_\mathrm{d} = 0$ (figure 3). This is a necessary, though not sufficient, test for the Ricatti matrix method; if it is to be useful and effective, it should lead to the expected results for this case without any erring. When there is no kind of flux at all, $f_\mathrm{s} = f_\mathrm{d} = 0$, we have only a four-site ring connected to the leads. An electron incident from the left lead is expected to pass to the right lead through the ring whenever its energy is, if the coupling t_0 between the leads and the ring is sufficiently small, approximately equal to the eigenenergies E_n of the isolated four-site ring. This should be so because the smallness of the coupling t_0 and the fact that there exists no prescribed interaction together can induce only an indiscernible change in the eigenenergies of the ring. Furthermore, again because of the absence of any interaction, we expect the transmissions at these eigenvalues to be perfect, i.e., $T(E_n) \approx 1$. Recalling that the eigenenergies of an N-site isolated ring is given, in the nearest-neighbour tight-binding scheme, by $E_n = -2t' \cos(2n\pi/N)$ with $n = 1, 2, \ldots, N$, we expect, for our system, the $T(E)$-curve to have four perfect transmissions, symmetric around the origin of the energy axis, at energies $E \approx \pm 1.0$ and 0.0 (doubly degenerate). All these expected features are clearly illustrated in figure 3(a).

What happens if we now allow a nonzero static flux, of strength f_s, to thread the ring? This time the eigenenergies of an N-site isolated ring are modified to $E_n = -2t' \cos[2(n + f_\mathrm{s})\pi/N]$,

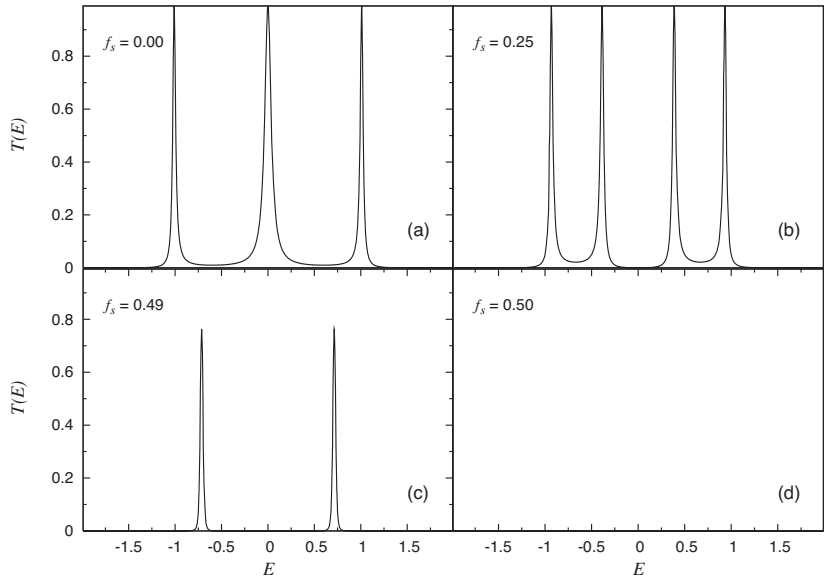

Figure 3. The total transmission, equation (41), in the absence of electron–phonon interaction for four different static flux strengths, without any dynamic flux. The Hamiltonian parameters used are $t = 1.0$, $t' = 0.5$, $t_0 = 0.2$, $\omega = 0.3$. Note that the total transmission is zero in (d), irrespective of the energy.

again with $n = 1, 2, \ldots, N$. Then for $f_s = 0.25$, for example, we anticipate four perfect transmissions, but still no prescribed interaction, at energies $E \approx \pm 0.38$ and ± 0.92, as shown in figure 3(b). We note that a nonzero flux lifts the degeneracy of the eigenenergy $E_1 = E_3 = 0.0$ seen in the previous case of zero flux (figure 3(a)). The form of the eigenenergy equation for this case suggests that at $f_s = 0.5$, for instance, we should see two perfect transmissions, both of them doubly degenerate, at energies $E \approx \pm 1/\sqrt{2} \approx \pm 0.71$. As is seen in figure 3(d), it turns out, however, that, at $f_s = 0.5$, no transmission peak at all appears, regardless of the electron energy. This phenomenon is referred to as total reflection [31–33], and is due to the perfect interference taking place when the electron wavefunctions in the upper and lower parts of the ring are completely cancelled at the point of the ring–lead junction, site $j = 2$ in our system; the condition for such a total reflection in an AB ring is that the flux strength f_s be half-integral numbers [33]. This feature is more striking than may be perceived at first glance. Except for the total reflection occurrences, we now realize that a four-site ring threaded by a constant magnetic flux always possesses four eigenenergies, though some of them may be degenerate; corresponding to them are four perfect transmissions. This fact holds even when there happens to be a slight shift in f_s from a half-integral value at which a total reflection takes place. In figure 3(c) is seen an example of such a situation where the two nearly perfect transmission peaks which are lost in figure 3(d) are recovered for a representative value of $f_s = 0.49$ around $E \approx \pm 0.71$. These are not literally perfect transmissions since the value $f_s = 0.49$ is too close to the 'singular' point $f_s = 0.5$, though it acts consummately well to make the missing transmission peaks reappear.

The results presented in the preceding paragraphs open up useful possibilities for an AB ring with a *static* flux to be utilized as a switch in the not-too-distant future quantum electronics applications. For example, the 'circuit' associated with figure 3(a) can be used as a three-way switch in the sense that it allows a current to flow only three specific electron energies;

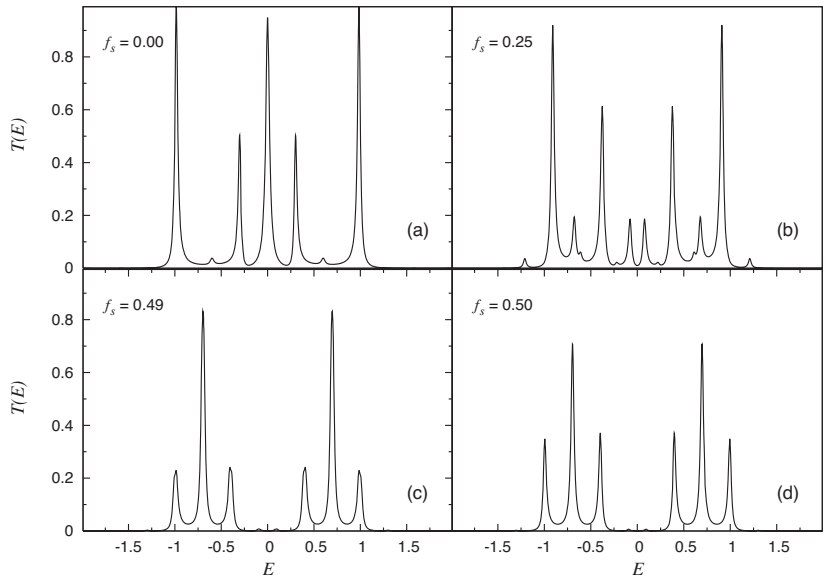

Figure 4. The same as figure 3, but with a dynamic flux of strength $f_{\rm d} = 0.2$. Note, in (d), the reappearance of the main transmission peaks which were lost in figure 3(d).

otherwise it blocks the current. It is to be noted that the width of transmission peaks may be adjusted according to the magnitude of the coupling t_0 between the ring and the leads. Hence the energy range in which the current flows may be predetermined in compliance with particular needs, and the switch's oversensitivity to the energy is thus prevented. Likewise, the circuits associated with figures 3(b) and (c) may be exploited as a four-way and two-way switch, respectively. The circuit associated with figure 3(d), along with figure 4(d), seems to offer a similar switch behaviour, this time according to the magnitude of the flux strength $f_{\rm s}$. Its oversensitivity to $f_{\rm s}$ might not permit this circuit to operate properly as a switch, however.

A nonzero dynamic flux is now allowed in order to take a close look at the photon-assisted tunnelling taking place in the present AB system (figure 4). We are still excluding electron–phonon interaction, $\kappa = 0$. We begin with figure 4(a), the case in which we apply only a dynamic flux, without a static flux. What would we expect if we were dealing with a simpler system in which there was a single site at the central region, instead of an AB ring, that was driven by a time-periodic potential of period ω? The interaction with the central site would then cause the electron to gain or lose energy quanta ω, or, say, *photons*, and the scattered electron would have an energy dictated by the Floquet states $E \pm n\omega$. As a result, we would expect that the central transmission peak (here we assumed that the central onsite energy was zero) had *satellite* peaks appearing symmetrically at positions $E \approx \pm m\omega$, and that their number would be increasing with the increasing dynamic potential strength, but with decreasing heights at the same time. We now return to our present problem. Although the conceptual problem above seems somewhat different in nature, there is no reason not to expect the same features to come into view, and similar satellite peaks might be expected to appear at energies $E \approx E_n \pm m\omega$, where E_n is the eigenenergy of the isolated AB ring without a dynamic flux. Loosely speaking, these additional satellite peaks represent the emission or absorption of a photon; hence that part of the paper's title 'photon-assisted tunnelling' finds its meaning. (The reader is also referred to the continuum AB ring cases [29, 32–34] to observe similar characteristics.) We indeed

see these expected behaviours in figure 4(a): there appear four satellite peaks *only* around the central transmission peak, symmetrically distributed at locations $E \approx \pm\omega$ and $E \approx \pm 2\omega$; the closer to the main peak a satellite peak is, the bigger its height is. We do not see more satellite peaks because the strength of dynamic flux is too small for the electron to be scattered to (absolutely) higher Floquet states. We notice the slight decrease in the height of the central transmission peak, an expected behaviour, since this time, contrary to the previous bare and only static flux cases, we now *do* have electron–photon interaction; we no longer see any perfect transmission.

The only seeming peculiarity about figure 4(a) with the results just presented is that we do not observe any satellite peaks around the outermost main transmission peaks; they remain *stiff*, even for a stronger dynamic flux (not shown). (This happening is exclusive to figure 4(a), not seen in figures 4(b)–(d), among the cases considered in this work.) Although the concrete reason for this somewhat unexpected outcome remains elusive for the time being; a plausible account might be provided by analysing the phase of the electron wave, like that in the analogous continuous AB ring [32, 33]. To do so we make use of the eigenenergy formula for an isolated N-site ring in the nearest-neighbour tight-binding scheme, introduced before, written as $E_n = -2t' \cos(2n\pi/N) = -2t' \cos(k_n \ell) = -2t' \cos(2\pi\ell/\lambda_n)$, where λ_n is the characteristic wavelength. Here we introduced ℓ being the quarter circumference of the ring, which we take as being unity in this work; it is the nearest-neighbour distance between any two sites in the ring. With $t' = -0.5$ and $N = 4$ for the system under study, it becomes $E_n = -\cos(n\pi/2) = -\cos(2\pi\ell/\lambda_n)$. Therefore, the stiff peaks under question are located at energies $E_2 \approx 1.0$ and $E_4 \approx -1.0$, as shown in figure 4(a), which correspond respectively to electron wavefunctions with wavelengths $\lambda_2 = 2\ell$ and $\lambda_4 = \ell$. On the other hand, the position of the central transmission peak is $E_1 = E_3 \approx 0.0$ (doubly degenerate), corresponding to $\lambda_1 = 4\ell$ or $\lambda_3 = 4\ell/3$. We now realize that whenever the wavelength λ happens to be an integral multiple of ℓ, the nodes of the electron wavefunction and the sites of the ring are perfectly matched. Based on this fact, we may surmise that it is somehow difficult for a dynamic flux to disturb an electron wavefunction with a wavelength matched perfectly to the sites of the ring. Consequently, it is highly likely that the cases of λ_1, λ_2, and λ_4 (indistinguishable in figure 4(a) from the λ_3 case) do not give rise to any satellite peaks; the additional channels for the corresponding main transmission peaks cannot be opened even under a dynamic flux with a stronger strength. It is only the $\lambda_3 = 4\ell/3$ case, with unmatched wavelength, that yields satellite peaks. The reader should notice that, contrary to the analogous continuous AB ring where the perfect matching takes place only in the two junction points of the ring and the leads [32, 33], in the system under study, shown in figure 1, perfect matching occurs at all four sites, i.e., even at sites 1 and 3.

All the presumed features, most of which are seen in figure 4(a), are markedly distinguished in figures 4(b)–(d), where we also have a static flux in addition to the already available dynamic flux. Each main transmission peak now possesses its own satellite peaks, although, in figure 4(b), it seems at first sight fairly difficult to determine which satellite peak is the offspring of which main transmission peak. We are now well aware of the substantial reduction of the main transmission peaks in all graphs. Because of the dynamic flux with not-so-strong strength f_d, only the first-order Floquet excitations are clearly seen; the second-order ones are also visible in figure 4(b), but they are barely discernible in figures 4(c) and (d). The most striking of all is demonstrated in figure 4(d) where there appear not only the expected satellite peaks, but also the main transmission peaks, at $E \approx \pm 0.71$, which were missing in figure 3(d), because of the half-integral f_s value leading to a perfect reflection. As we mentioned above, even a very small deviation from $f_\mathrm{s} = 0.5$ destroys the perfect reflection, giving rise to a significant change in the total transmission. It plainly follows from figure 4(d)

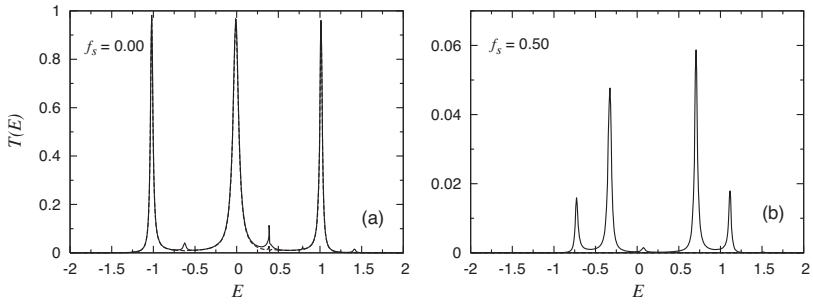

Figure 5. The total (solid lines) and elastic (dashed lines) transmissions at zero temperature in the presence of electron–phonon interaction, without a dynamic flux. We choose $\kappa = 0.1$ and $\Omega = 0.4$; the remaining parameters are the same as those in figure 3. It is to be noticed that the elastic transmission is zero in (b); hence, no graph with dashed line is visible there. Also, the scales of the vertical axes are different.

that although a static flux with a half-integral strength f_s is applied, perhaps to avoid any transmission resonance, the dynamic flux keeps open at the same the main transmission channels as well as satellite pseudochannels. The fact of matter is that this special occurrence proves the oversensitivity of the circuit associated with figure 3(d) for the only-static-flux case, as we pointed out above.

We next study the cases in which electron–phonon interaction is considered with and without a static flux, but excluding, for the moment, any dynamic flux, $f_d = 0$; we investigate the total and elastic tunnelling through the AB ring at zero temperature. Here we mean with 'elastic scattering' that the number of phonon quanta excited on each of the central sites of the ring are zero both before and after the scattering, because of the zero temperature. Figure 5 shows the total and elastic transmissions as a function of the electron energy for the special cases $f_s = 0.0$ and 0.5. We first observe that the demonstrated features are entirely similar to those of Haule and Bonča [20], proving the consistency of both methods. It seems sufficient to provide only a brief summary. It follows from figure 5(a) that satellite resonances are located at $E \approx E_n + m\omega$, where m is a *positive* integer and E_n is, in general, the eigenenergies for an isolated N-site ring in the nearest-neighbour tight-binding scheme; to repeat, $E_n = -2t' \cos(2n\pi/N)$. These additional satellite peaks signify, this time, phonon emissions or absorptions; hence follows the first part of the paper's title 'phonon-assisted tunnelling.' Because no phonon exists for absorption at the sites of the ring before the scattering, there is no satellite peak, corresponding to phonon absorption, on the left of the main transmission peaks, so the m that appears in the above formula is positive. We see only two satellite peaks, corresponding to phonon emission, on the right of the central transmission peak (though the second one requires a powerful eye) and only one on the right of the outermost main transmission peaks, since the strength κ of the electron–phonon coupling is too small for the electron to cause more phonon emissions. We also note the slight decrease in the height of the main transmission peaks, similar to that encountered above in the photon-assisted tunnelling. As expected, with increasing κ value, the number of satellite peaks increases, and the decrease in the heights of the main transmission peaks becomes more pronounced (not shown). Finally, although the difference is hardly discerned, a comparison of the total and elastic transmissions in figure 5(a) reveals that there is always a significant probability for an electron to cause higher-order phonon emissions, no matter how small the coupling strength κ is.

As we mentioned before, in the absence of electron–phonon interaction, the total reflection phenomenon, i.e., zero transmission, is encountered for a static flux of strength $f_s = 0.5$,

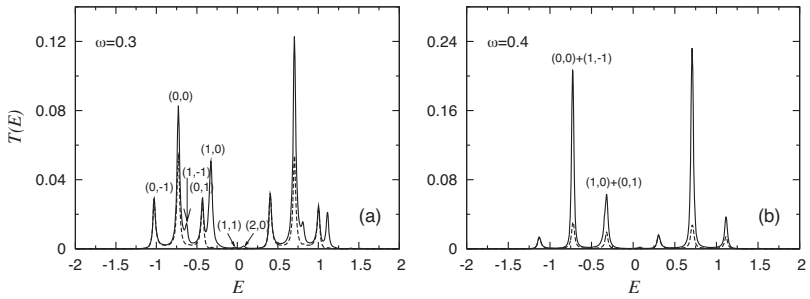

Figure 6. The total (solid lines) and elastic (dashed lines) transmissions at zero temperature in the presence of electron–phonon and electron–photon interactions at two different Floquet frequencies. The pair (p, q) in (a) designates the number of excited phonon, p, and photon, q, quanta. We choose $\Omega = 0.4$, $f_s = 0.5$, $f_d = 0.05$, and $\kappa = 0.1$; the remaining parameters are the same as those in figure 3. It is to be noticed that the scales of the vertical axes are different.

irrespective of the electron energy. The inclusion of electron–phonon interaction gives rise to a finite, though small, total transmission, as is seen in figure 5(b). Noting that the elastic contribution is exactly (within the numerical precision imposed) zero in this case, we can draw the conclusion that all the contributions to the total transmission in this case come only from inelastic processes (i.e., sequential phonon emissions and re-absorptions) via the additional phonon channels [19].

We lastly work out the case in which the effects of both electron–phonon and electron–photon interactions on the transmission properties of the system are investigated. Put in an other way, all the parameters of the system are now at work; therefore, all the previously observed individual effects are expected to come additively together to reshape the transmission curve. Figure 6(a), where we plot the total and elastic transmissions as a function of the electron energy, certifies these expectations. For a better appreciation, we designate by the pair (p, q) a general phonon–photon channel, where p (q) is the number of excited phonon (photon) quanta on any site of the AB ring. We focus on the left main transmission peak and its satellite peaks in figure 6(a). If only a static flux of strength $f_s = 0.5$ were applied, we would see a perfect reflection, figure 3(d). As is seen in figure 4(d), the inclusion of a oscillating dynamic flux then recreates the missing main transmission peaks, and creates the associated satellite peaks. In figure 6(a), the left main transmission peak is indicated by channel $(0, 0)$, and the satellite peaks by $(0, -1)$ and $(0, 1)$, which refer respectively to the pure absorption and pure emission of one photon quantum. We note from the behaviour of the dashed line that these two satellite peaks are due to elastic photon absorption–emission processes. The satellite peaks $(1, 0)$ and $(2, 0)$ indicate pure one- and two-phonon inelastic emission processes, respectively. Via the electron–photon interaction, these pure phonon processes are accompanied by the additional hybrid satellite peaks; examples are the peaks $(1, 1)$ and $(1, -1)$, which are at a distance $\pm\omega$ from the pure phonon peak $(1, 0)$. The trend should now be obvious; to sum up, the presence of both interactions creates many new channels, or states, within the band of the electron, whose locations are given by $E \approx E_n + p\Omega \pm q\omega$, where E_n gives the eigenenergies of an isolated four-site ring, for the present study, in the nearest-neighbour tight-binding scheme.

We consider, finally in this work, the case in which we have the same numerical magnitude for the frequency of the time-periodic flux and that of the phonon field, $\omega = \Omega = 0.4$. As is now readily expected, the positions of the satellite photon peaks coincide with those of the phonon peaks on the *right* side of the main transmission peaks, as figure 6(b) clearly illustrates. We notice how beautifully the channels $(1, 0)$ and $(0, 1)$ in figure 6(a) combine into one *phonon–*

photon satellite peak in figure 6(b), which now has a significantly enhanced height. Perhaps more interestingly, since the photon satellite peak $(1, -1)$ coincides with it, the height of the main transmission peak $(0, 0)$ is augmented by a factor of more than two. The results presented in figure 6 constitute a compact summary of the present work; hence follows readily the paper's title 'phonon–photon-assisted tunnelling.'

4. Summary and conclusions

We investigate the phonon–photon-assisted tunnelling through a four-site AB ring, whose sites are coupled to electron–phonon interaction, which is threaded by a time-periodic flux. We offer the use of the Ricatti matrix method, a nonperturbative numerically exact method to obtain the transmission properties of the system under question. We combine the Floquet scattering approach of Shirley and Sambe [23, 24] (to deal with the time-periodic flux), the mapping scheme of Bonča *et al* [19, 20] (to handle electron–phonon interaction), and, in turn, the Ricatti ratio method of Heinrichs and Faizabadi *et al* [27, 28] (to prune the system) into a single effective matrix method. As a whole, the method presented in this work makes the interacting Hamiltonian transform to an effectively noninteracting one, and it thus permits the Floquet theory to be applicable to a system even with phonon degrees of freedom.

After a description of the problem, its formulation along with a detailed derivation of the method to solve the time-dependent Schrödinger equation associated with the total Hamiltonian of the system are given. In order to test the method, the tunnelling under the effect of only a static flux without electron–phonon interaction is first considered and all the expected outcomes are recovered. It is seen that a static flux lifts the degeneracy of the eigenenergies of the ring, and moves or combine these eigenenergies. At a static flux of half-integral strength f_s, the total reflection phenomenon is observed irrespective of the electron energy. The missing main transmission peaks are observed to reappear when even there is a very small shift in f_s from a half-integral value. These results imply that such an AB system with only a static flux might be fully exploited as a nanoswitch in near-future quantum electronics. A dynamic flux is then applied to the system, again without electron–phonon interaction. The phonon-assisted tunnelling is seen at work and there appear satellite photon peaks symmetrically around main transmission peaks. In a special case, some main transmission peaks remain stiff, i.e., the expected photon satellite peaks around them do not appear, even for a stronger dynamic flux. It is conjectured that whenever the nodes of the electron wavefunction and sites of the ring are perfectly matched, the electron wavefunction is unwilling to give birth to any satellite photon peak. It is later noticed that, although a static flux with a half-integer strength is applied, a dynamic flux keeps open the lost main transmission channels as well as satellite photon channels. Next, electron–phonon interaction is considered at zero temperature with and without static flux, excluding any dynamic flux. All the previously reported literature results are recovered, proving the accuracy and efficiency of the present method. Phonon satellite peaks signifying phonon emission and absorption precesses are observed. It is found that there is always a significant probability for an electron to cause high-order phonon emissions, no matter how small the electron–phonon coupling strength is. It is seen that the inelastic processes of sequential phonon emissions and re-absorptions play a substantial role in forming the transmission properties of the system. Finally, both electron–phonon and electron–photon interactions are included, and all the previously observed individual effects are seen to come additively together to affect the system. The inclusion of both interactions creates many additional channels, or satellite peaks, or states within the band of the electron, whose locations are dictated by $E \approx E_n + p\Omega \pm q\omega$, where E_n is, in general, the eigenenergies of an isolated N-site ring, in the nearest-neighbour tight-binding scheme. In the special case in

which frequencies of the time-periodic flux and phonon field are equal in magnitude, satellite phonon and photons peaks coincide and thus enhance the effect of each other. Similarly, a main transmission peak may merge with a photon and/or phonon satellite peak, leading to a much more strong transmission probability at a special electron energy which can easily be adjusted by tuning the strength of static flux. It would be interesting to study, with the use of the method presented in this work, a double AB ring system whose rings are threaded by a couple of out-of-phase time-periodic dynamic fluxes so that one practically obtains a quantum electron pump system. It would be even more appealing, and thought-provoking, to include electron–phonon interaction in such an electron pump. We are currently working on both.

Acknowledgment

This work was supported by the Korea Research Foundation, Grant No. KRF-2006-0409-0060.

References

[1] Datta S 1995 *Electronic Transport in Mesoscopic Systems* (Cambridge: Cambridge University Press)
[2] Yacoby A, Heiblum M, Mahalu D and Shtrikman H 1995 *Phys. Rev. Lett.* **74** 4047
[3] Ji Y, Heiblum M, Sprinzak D, Mahalu D and Shtrikman H 2000 *Science* **290** 779
[4] Kobayashi K, Aikawa H, Katsumoto S and Iye Y 2002 *Phys. Rev. Lett.* **88** 256806
[5] Keyser U F, Borck S, Haug R J, Bichler M, Abstreiter G and Wegscheider W 2002 *Semicond. Sci. Technol.* **17** L22
[6] Heath J R and Ratner M A 2003 *Phys. Today* **56** 43
[7] Park H, Park J, Lim A K L, Anderson E H, Alivisatos A P and McEuen P L 2000 *Nature* **407** 57
[8] Fujisawa T, Oosterkamp T H, van der Wiel W G, Broer B W, Aguado R, Tarucha S and Kouwenhoven L P 1998 *Science* **282** 932
[9] Chen J, Reed M A, Rawlett A M and Tour J M 1999 *Science* **286** 1550
[10] Dong B, Cui H L and Lei X L 2004 *Phys. Rev.* B **69** 205315
[11] Wingreen N S, Jacobsen K W and Wilkins J W 1988 *Phys. Rev. Lett.* **61** 1396
[12] Wingreen N S, Jacobsen K W and Wilkins J W 1989 *Phys. Rev.* B **40** 11834
[13] Foa Torres L E F, Pastawski H M and Makler S S 2001 *Phys. Rev.* B **64** 193304
[14] Pastawski H M, Torres L E F F and Medina E 2002 *Chem. Phys.* **281** 257
[15] Ness H and Fisher A J 2002 *Chem. Phys.* **281** 279
[16] Galperin M, Ratner M A and Nitzan A 2004 *J. Chem. Phys.* **121** 11965
[17] Asai Y 2004 *Phys. Rev. Lett.* **93** 246102
[18] Frederiksen T, Brandbyge M, Lorente N and Jauho A P 2004 *Phys. Rev. Lett.* **93** 256601
[19] Bonča J and Trugman S A 1995 *Phys. Rev. Lett.* **75** 2566
[20] Haule K and Bonča J 1999 *Phys. Rev.* B **59** 13087
[21] Platero G and Aguado R 2004 *Phys. Rep.* **395** 1
[22] Kohler S, Lehmann J and Hänggi P 2005 *Phys. Rep.* **406** 379
[23] Shirley J H 1965 *Phys. Rev.* **138** B979
[24] Sambe H 1973 *Phys. Rev.* A **7** 2203
[25] Moskalets M and Büttiker M 2002 *Phys. Rev.* B **66** 205320
[26] Lehmann J, Kohler S, May V and Hänggi P 2004 *J. Chem. Phys.* **121** 2278
[27] Heinrichs J 2002 *Phys. Rev.* B **65** 075112
[28] Faizabadi E and Ebrahimi F 2004 *J. Phys.: Condens. Matter* **16** 1789
[29] Bulgakov E N and Sadreev A F 1995 *Phys. Rev.* B **52** 11938
[30] Lubin D, Gefen Y and Goldhirsch I 1990 *Phys. Rev.* B **41** 4441
[31] Büttiker M, Imry Y and Azbel M Y 1984 *Phys. Rev.* A **30** 1982
[32] Yi J, Wei J H, Hong J and Lee S I 2001 *Phys. Rev.* B **65** 033305
[33] Park W and Hong J 2004 *Phys. Rev.* B **69** 035319
[34] Shin D and Hong J 2005 *Phys. Rev.* B **72** 113307